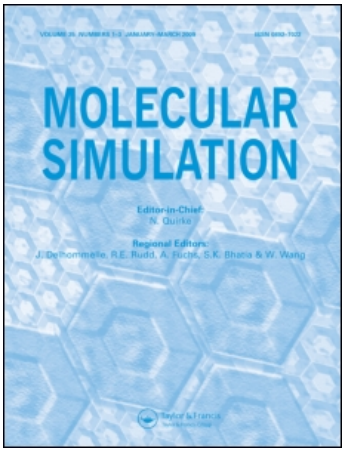

Molecular Simulation
Publication details, including instructions for authors and subscription information:
http://www.informaworld.com/smpp/title~content=t713644482

Comparison of perfluoropolyethers and *n*-alkanes under shear via nonequilibrium molecular dynamics simulation

B. Jiang[a]; J. M. Kim[a]; D. J. Keffer[a]; B. J. Edwards[a]
[a] Department of Chemical and Biomolecular Engineering, The University of Tennessee, Knoxville, TN, USA

To cite this Article Jiang, B. , Kim, J. M. , Keffer, D. J. and Edwards, B. J.(2008) 'Comparison of perfluoropolyethers and *n*-alkanes under shear via nonequilibrium molecular dynamics simulation', Molecular Simulation, 34: 2, 231 — 242
To link to this Article: DOI: 10.1080/08927020801993362
URL: http://dx.doi.org/10.1080/08927020801993362

Molecular Simulation
Vol. 34, No. 2, February 2008, 231–242

Taylor & Francis
Taylor & Francis Group

Comparison of perfluoropolyethers and *n*-alkanes under shear via nonequilibrium molecular dynamics simulation

B. Jiang, J.M. Kim, D.J. Keffer* and B.J. Edwards

Department of Chemical and Biomolecular Engineering, The University of Tennessee, Knoxville, TN, USA

(Received 11 December 2007; final version received 13 February 2008)

The structural, energetic and rheological properties of seven short-chain perfluoropolyethers (PFPEs) under planar Couette flow have been investigated through nonequilibrium molecular dynamics (NEMD) simulation. The full parameter set of a revised universal force field (A.K. Rappe et al., *UFF, a full periodic table force field for molecular mechanics and molecular dynamics simulations*, J. Am. Chem. Soc. 114 (1992), p. 10024) is presented for linear PFPEs, allowing for multiple types of fluorine atoms depending upon their local environment (B. Jiang et al., *Comparison of rheological properties of short-chain PFPEs through simulation and experiment*. Mol. Simul. 33 (2007), p. 871). The NEMD simulations quantitatively reproduce experimental zero-shear-rate viscosities for five PFPEs with varying molecular architectures. Rheological properties and structural variations of PFPEs are investigated as functions of flow strength, temperature and chain architecture. We find the following general relationships between PFPE architecture and viscosity: (i) longer chain lengths increase the viscosity, (ii) ether linkages in the backbone decrease the viscosity and (iii) longer $(CF_2)_n$ units between ether linkages increase the viscosity. These effects are all explained in terms of chain flexibility. Additionally, we report the structural and rheological properties of four short-chain PFPEs with identical monomeric units but with different chain lengths using NEMD simulation of planar Couette flow. We explain the behaviour of the longer PFPEs due to the increased relative flexibility of longer chains over shorter chains. Finally, we provide a quantitative comparison of the structural and energetic properties of relatively rigid PFPEs and relatively flexible alkanes as a function of chain length. In general, alkanes respond to the flow field with a combination of alignment and extension. PFPEs respond with greater alignment but less extension. An increase in chain length enhances the degree of alignment at high shear rates and enhances the degree of extension at intermediate shear rates.

Keywords: perfluoropolyether; lubrication; viscosity; rheology; nonequilibrium molecular dynamics simulation

1. Introduction

In the past decades, perfluoropolyethers (PFPEs) have been used as high performance lubricants in diverse applications such as oil service, military and aerospace, arctic and space exploration at both relatively high and low temperatures and under normal and severe operation conditions because of their chemical inertness, thermal stability, lower pour point and inflammability [1,2]. For example, Fomblin and Krytox are widely used as lubricants in magnetic recording media [3,4].

A significant number of studies have been conducted with the aim of characterising PFPE lubricants experimentally and computationally. Snyder et al. applied the reciprocating and four-ball tribometers to evaluate the performance of different types of commercially available PFPEs under dynamic bearing conditions [1,5,6]. Their research described structure/property relationships at the macroscopic level, such as the destabilising effect of an $-OCF_2O-$ group. Several research groups studied the rheological properties of PFPE lubricants [7–14]. A coarse-grained bead-spring model was used by Jhon et al. [10,15] and Li et al. [16] to investigate the structural transformations in a nanoscale film with respect to the effect of the functional end groups on the rheological properties of PFPEs. Li et al. [3,17,18] developed a united-atom potential model based on *ab initio* quantum mechanics calculations for the short-chain perfluoroalkanes and perfluoroethers, and applied it to study the phase diagram through Gibbs ensemble Monte Carlo simulations; these reproduced well the experimental critical properties of perfluoromethylpropyl ether. Explicit atom potentials were also applied by Koike [11] and Kamei et al. [19] to different types of PFPEs confined between two rigid surfaces of different lattices. Viscosities and friction coefficients were reported across a range of temperatures. Senapati et al. [20] performed molecular dynamics simulations to study the structural properties of carboxylate PFPE in supercritical carbon dioxide.

*Corresponding author. Email: dkeffer@utk.edu

ISSN 0892-7022 print/ISSN 1029-0435 online

DOI: 10.1080/08927020801993362
http://www.informaworld.com

In previous studies [21,22], we used a combination of nonequilibrium molecular dynamics (NEMD) simulation and experimental characterisation to study the rheological behaviour of PFPEs under planar couette flow (PCF) as a function of strain rate, temperature, and chain architecture. We chose to use an explicit atom potential since previous work had demonstrated that while united-atom models can satisfactorily generate transport properties for hydrocarbons, they introduce significant errors for fluorocarbons due to the increased size of the fluorine atom [23]. In order to reproduce, both qualitatively and quantitatively, the experimentally observed relationship between PFPE architecture and zero-shear-rate viscosity, we modified the universal force field (UFF) [24] potential to accommodate different types of fluorine atoms, depending on the local environment. The modification involved very modest (less than 15% changes) in the non-bonded F interaction parameters. This adjustment is consistent with the work of Li et al., who similarly found it necessary to define different fluorine atom potentials in PFPEs when using molecular simulation to predict vapour–liquid equilibria [3,17,18]. The revised UFF potential of Refs. [21,22] enabled the NEMD simulations to reproduce the experimentally observed trends in viscosities.

In this study, we examined three additional features of PFPEs undergoing shear flow. First, we complete the parameterisation of the modified potential for linear PFPEs by synthesising and simulating an additional PFPE molecule with an additional type of fluorine atom, which is the only remaining possibility for the linear PFPEs that we have not previously investigated. Second, we use the full potential in NEMD simulations to study four short-chain PFPEs with similar monomeric units but with different chain lengths undergoing PCF. Third, we explain the relationship between PFPE architectural elements and the resulting viscosity through arguments regarding chain flexibility. To understand fully the effect of chain flexibility, we compare the energetic and structural properties of PFPEs with more flexible chain molecules, namely linear alkanes of similar backbone length.

Herein, we report NEMD simulation results for seven PFPE compounds and two linear alkanes. The structures of the seven PFPE compounds are summarised in Table 1. All PFPE compounds, except compound 4, can be represented as variations of the generic structure

$$CF_3(CF_2)_k - [O(CF_2)_n]_m - O(CF_2)_kCF_3,$$

where m represents the number of monomeric units in the chain, n is the number of CF_2 units in each monomer, and k is the number of CF_2 units in each end group. Thus, m quantifies the chain length, n quantifies the monomer size, and k determines the size of the functional end group. In this study, m assumes values of 2, 3, 5 and 7, n assumes values of 1, 2 and 3, and k assumes values of 0 and 1. Compound 4 is a variation of compound 2, in which an $-OCF_2-$ monomer has been inserted into the middle of the chain.

The effect of chain length on energetic, structural, and rheological properties of chain molecules under flow has received substantial attention for linear alkanes and short-chain polyethylene liquids. Previous molecular dynamics studies [25–31] of normal alkanes revealed rich structural information under various types of applied flow fields, furthering our understanding of the structure–properties of polymers at the atomic scale. These previous studies characterised the energetic, structural and rheological properties as functions of strain rate, and examined the dependence of viscosity, the various intra- and intermolecular contributions to the potential energy, the end-to-end distance, the radius of gyration and the conformation tensor on strain rate. In this work, we present analogous information for the relatively much stiffer PFPEs of different chain lengths. We compare the NEMD simulations of the PFPE compounds with those from simulations of two *n*-alkanes of similar lengths, hexadecane ($C_{16}H_{34}$) [27,32,33] and tetracosane ($C_{24}H_{50}$) [32,34,35].

2. Experimental procedure

The first five PFPEs listed in Table 1 were synthesised by the direct aerosol fluorination process developed by Adcock et al. [36–38]. The detailed information on synthesis, separation and purification can be found in the cited references. Relevant to this work, we used the

Table 1. Summary of PFPE structures and architectural elements.

#	Chemical formula	Structure	Backbone atoms	Architectural elements
1	$C_8F_{18}O_4$	$CF_3-[O(CF_2)_2]_3-OCF_3$	12	Base ($m = 3$)
2	$C_6F_{14}O_3$	$CF_3-[O(CF_2)_2]_2-OCF_3$	9	Chain length ($m = 2$)
3	$C_8F_{18}O_3$	$CF_3CF_2-[O(CF_2)_2]_2-O\ CF_2CF_3$	11	End group
4	$C_7F_{16}O_4$	$CF_3O(CF_2)_2OCF_2\ O(CF_2)_2OCF_3$	11	OCF_2O
5	$C_8F_{18}O_3$	$CF_3-[O(CF_2)_3]_2-OCF_3$	11	OC_3F_6O
6	$C_{12}F_{26}O_6$	$CF_3-[O(CF_2)_2]_5-OCF_3$	18	Chain length ($m = 5$)
7	$C_{16}F_{34}O_8$	$CF_3-[O(CF_2)_2]_7-OCF_3$	24	Chain length ($m = 7$)

measured densities of these compounds at 293 K to determine the densities applied in the NEMD simulations. The densities at other temperatures were estimated using the coefficient of thermal expansion, $0.001°C^{-1}$, reported by Bell et al. [2]. The last two PFPE compounds listed in Table 1 were not synthesised. Their densities were estimated through the linear interpolation of densities for compounds $C_8F_{18}O_4$ and $C_6F_{14}O_3$, and the densities of similar molecular structures with high molecular weights, as reported by Solvay & Solexis, Inc. (http://www.solvaysolexis.com/). The densities used in this work are listed in Table 2. The viscosities for all compounds that were experimentally synthesised were measured with the Cannon–Manning Semi-Micro Viscometer, manufactured by Cannon Instrument Co.

3. Nonequilibrium molecular dynamics simulation

3.1 Interaction potentials

The starting point for the potential model used in the work of PFPEs is the UFF developed by Rappe et al. [24]. The detailed information on the UFF potential and how we perturbed the UFF potential to describe faithfully the relationship between viscosity and molecular architectures of PFPEs can be found in previous publications [21,22]. Here we summarise briefly as follows. The UFF potential consists of contributions from: (i) bond stretching, (ii) bond bending, (iii) dihedral bond torsion and (iv) intra- and inter-molecular non-bonded interactions via a Lennard-Jones 12-6 potential. The intramolecular non-bonded interactions involve the atoms separated by three or more bonds. UFF potential does not explicitly include partial charges, whose contributions are included in non-bonded interactions. The revised UFF potential of [22] changed only the non-bonded parameters for the fluorine atoms according to the local environment. In this work, we assume the local environment to be completely defined by the atoms chemically bonded to the carbon atom of which the fluorine of interest is itself bonded.

Table 2. The densities (g/ml) of the seven PFPE compounds investigated in this work at different temperatures.

	T (K)				
No.	253	293	313	333	373
1	1.686	1.620	1.588	1.556	1.497
2	1.679	1.613	1.584	1.550	–
3	1.699	1.633	1.603	1.568	1.508
4	1.728	1.660	1.627	1.595	1.532
5	1.755	1.687	1.656	1.620	1.558
6	1.714	1.647	1.614	1.582	1.521
7	1.730	1.662	1.630	1.597	1.536

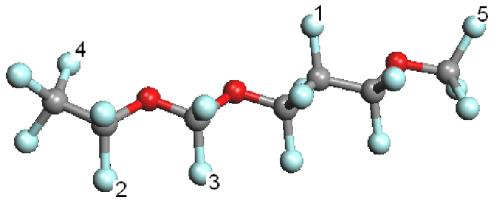

Figure 1. Types of fluorine atoms in linear PFPEs. The type of F atom is defined by the atoms to which the adjacent carbon is bound. There are five groups centered on C atoms: (1) CF_2C_2, (2) CF_2CO, (3) CF_2O_2, (4) CF_3C and (5) CF_3O. Note: Carbon atoms are grey, oxygen are red and fluorine are light blue.

The five types of fluorine atoms in linear PFPEs are shown in Figure 1. The five groups are labelled by the central C and the four additional atoms (including the F of interest) to which it is bound: (1) CF_2C_2, (2) CF_2CO, (3) CF_2O_2, (4) CF_3C and (5) CF_3O. This is a complete set of fluorine groups in linear PFPEs. The fluorine atom types in branched PFPEs were described previously [22]. Herein, all the simulations were performed using the revised UFF potential. The non-bonded interaction parameters are reported in Table 3, and should be used in an expression of the form

$$U_{ij} = \varepsilon_{ij}\left[\left(\frac{\sigma_{ij}}{r_{ij}}\right)^{12} - 2\left(\frac{\sigma_{ij}}{r_{ij}}\right)^{6}\right] \quad (1)$$

where U_{ij} is the pairwise interaction energy between atoms i and j, ε is the energetic well depth, σ is the collision diameter, and r_{ij} is the magnitude of the separation between atoms i and j.

3.2 Simulation technique

NEMD simulations were performed for all seven compounds presented in Table 1 by combining the SLLOD equations of motion with an atomic Nose–Hoover thermostat [39,40] and integration according to the multiple time-step method known as the reversible reference system propagator algorithm (r-RESPA) [41]. It is noteworthy that the type of thermostat may result in different extensions for the molecules at extremely high strain rates [42,43]. In our cases, the flow strength is relatively low, which means thermostat artifacts should be small. The large time step was 2 fs for the intermolecular non-bonded interactions and thermostat variables, and the small time step was 0.2 fs for the intramolecular interactions. In the NEMD simulations, PCF was imposed in the NEMD simulations to generate the trajectories of particles using the SLLOD [44] algorithm with the Lees–Edwards [45] boundary conditions.

The simulations contained 216 molecules, ranging from 4968 to 12,528 atoms, depending on the specific PFPE and chain length. A cut-off distance of 12.5 Å was

Table 3. Parameters of the non-bonded interaction for different types of fluorine atoms in the revised UFF potential.

Type	CF_3O	CF_2CO	CF_3C	CF_2O_2	CF_2C_2	F*
ε/k_B (K)	25.16	25.16	25.16	21.39	25.16	25.16
σ (Å)	3.224	3.100	3.100	3.193	3.05	3.36

Note: F* stands for fluorine atom in the original UFF.

used for all the Lennard-Jones non-bonded interactions. For each compound, an artificially high temperature, 673 K, was used to generate reasonable initial configurations efficiently using equilibrium molecular dynamics simulation. For the NEMD simulations, the equilibrated configurations were used as starting points. The duration of the simulations depended strongly on the strain rate, temperature, and chain length, all of which strongly influenced the time required to attain steady state. Simulation durations ranged from 25 to 130 ns. At the lowest shear rate for $C_{16}F_{34}O_8$ at 293 K, 70 ns of simulation time was necessary to attain steady state, which was carefully checked by monitoring the end-to-end distance, conformation tensor and the distribution functions of torsion and bending angles. Data were collected over a period of at least 10 ns after a steady state was attained, with sampling every 10 ps.

4. Results and discussion

4.1 The full parameters of the revised UFF potential for linear PFPEs

In previous work publications [21,22], we presented the parameters for the revised UFF potential with regard to the four types of fluorine atoms in linear PFPEs. With the addition of the fifth compound, $C_8F_{18}O_3$ (C_3O), which possesses the final type of fluorine atom in the CF_2C_2 group, we followed an analogous procedure to obtain the non-bonded interaction parameters for this type of fluorine atom based on the experimental viscosity at 293 K, and then predicted the viscosity at 333 K. The non-bonded interaction parameters for fluorine atoms in the revised UFF potential are presented in Table 3. The viscosities from experiments and simulations using the revised UFF potential are presented in Figure 2 and Table 4. The viscosities from simulations were obtained by averaging the values in the Newtonian linear regions. In the previous work [22], we discussed the relationship between viscosity and molecular architecture for the first four compounds. The viscosities of the first four compounds generally increase with the increasing number of atoms in the molecular backbones. The addition of ether linkages adds flexibility to the chain; in particular, the existence of OCO in $C_7F_{16}O_4$ leads to a much lower viscosity when compared to $C_8F_{18}O_3$, although both of them share the same number of atoms in their backbones.

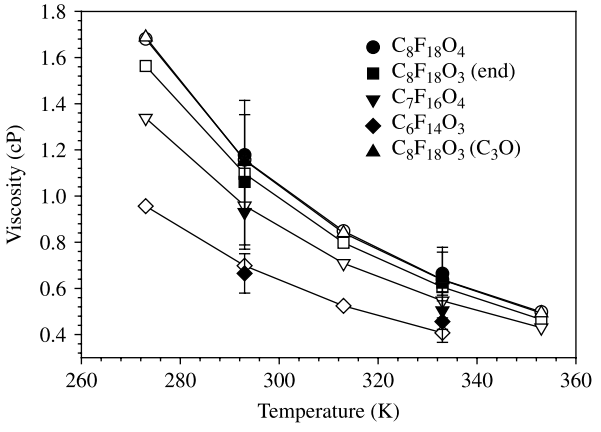

Figure 2. The zero-shear-rate viscosity vs. temperature for five compounds. The filled symbols represent results from NEMD simulations using the revised UFF potential, and the unfilled symbols represent experimental data.

The addition of the fifth compound allows us to put these observations in a new light. Because we now have chains with a single C atom between two ether links (the CO group in compound 4), two C atoms between two ether links (the C_2O groups in compounds 1 and 2), and three C between two ether links (the C_3O groups in compound 5), we can now judge the effect of monomer size. The larger the perfluorinated unit between the ether, the stiffer the chain and the higher the resulting viscosity. This can be seen most clearly by comparison of the fifth compound and the third compound, which have the same chemical formula, $C_8F_{18}O_3$. However, the fifth compound has C_3O groups and the third compound has C_2O groups. In this case, we have isolated the effect of monomer size. Furthermore, the fifth compound, $C_8F_{18}O_3$ (C_3O), unexpectedly shares the same experimental and simulated viscosities with $C_8F_{18}O_4$ (base) at almost all of the temperatures examined in Table 4. The fact that these two compounds have very similar viscosities can be seen as a balance between two opposing contributions. Since $C_8F_{18}O_4$ (base) and $C_8F_{18}O_3$ (C_3O) have 12 and 11 atoms in their molecular backbones, respectively, we would expect the longer

Table 4. The zero-shear-rate viscosities at various temperatures for five compounds. The viscosities from NEMD simulations using the revised UFF potential are in parenthesis.

	T (K)				
No.	273	293	313	333	353
1	1.68	1.16 (1.18)	0.85	0.64 (0.66)	0.50
2	0.96	0.70 (0.67)	0.52	0.41 (0.43)	–
3	1.56	1.10 (1.06)	0.80	0.61 (0.62)	0.47
4	1.34	0.96 (0.93)	0.71	0.55 (0.53)	0.43
5	1.69	1.16 (1.15)	0.84	0.64 (0.64)	0.49

base chain to have a higher viscosity. At the same time, the fifth compound has the longer monomer units (C_3O vs. C_2O) making it a stiffer chain, and suggesting that it should have the higher viscosity, all other things being equal. Taken in tandem, these two contributions virtually (and most likely, coincidentally) cancel each other out, leading to very similar viscosities.

The results from the revised UFF potential are consistent with the experimental data. Moreover, the adjustment of the non-bonded interactions of fluorine is modest. The fluorine in CF_3O have the largest effective diameter, 3.224 Å, and the fluorine atoms in CF_2C_2 have the smallest effective diameter, 3.05 Å, which is a variation of less than 6%. The energetic well depth was only changed for CF_2O_2; in all other groups, it was left at the UFF default value. In the case of CF_2O_2, the change was a reduction of 15%. Finally, the adjustment of the non-bonded interactions of fluorine atoms based on the local environment is well justified based on previous results [3,17,18].

4.2 The effect of chain length on rheological properties

In this section, we use the revised potential to investigate the role of chain length in PFPEs. Using compounds 1, 2, 6, and 7 in Table 1, we examined backbone lengths ranging from 9 to 24 atoms, while keeping the monomer unit and the end group constant.

4.2.1 Rheological properties from NEMD simulation

Shear viscosities from NEMD simulations using the revised UFF potential at varying shear rates and temperatures for $C_6F_{14}O_3$, $C_8F_{18}O_4$, $C_{12}F_{26}O_8$ and $C_{16}F_{34}O_8$ are shown in Figure 3. The plots primarily focus on the linear and nearly linear regions of shear rates, except for $C_{12}F_{26}O_8$ and $C_{16}F_{34}O_8$ at 293 K, since in the previous works [21,22] we presented the shear rate dependency for $C_6F_{14}O_3$ and $C_8F_{18}O_4$. All four compounds display a Newtonian plateau at low shear rates, where the time scale of the flow is long compared to that of the chains; hence a significant degree of chain stretching and alignment does not occur, and the shear stress is thus proportional to the applied value of the shear rate. For the longer two chains, $C_{12}F_{26}O_8$ and $C_{16}F_{34}O_8$, shear thinning behaviour is observed at high shear rates. Figure 3 also shows that the shear viscosities decrease with increasing temperature, as expected, since a higher temperature implies a lower potential energy (and higher kinetic energy) and reduced interactions

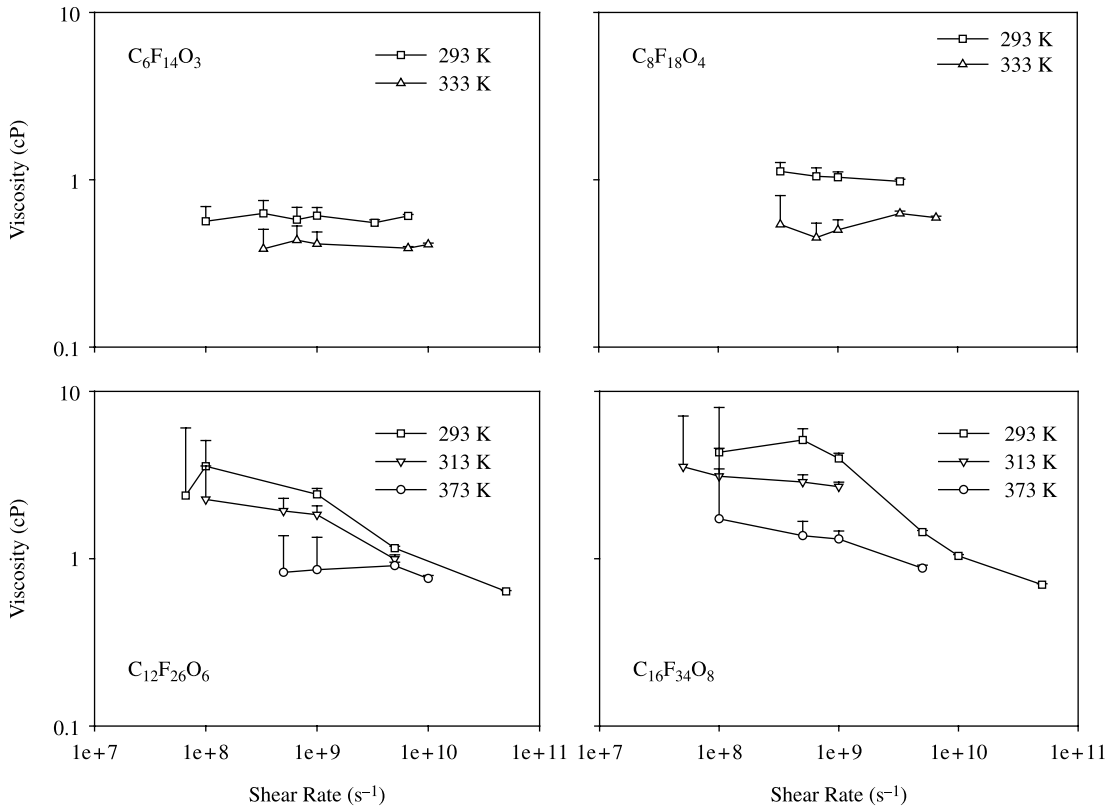

Figure 3. The shear viscosity vs. shear rate at different temperatures for compounds of various chain lengths: $C_6F_{14}O_3$, $C_8F_{18}O_4$, $C_{12}F_{26}O_6$, and $C_{16}F_{34}O_8$ using the revised UFF potential.

between intermolecular atomic units. The difference in shear viscosity between temperatures for $C_{12}F_{26}O_8$ and $C_{16}F_{34}O_8$ is clearly significant at low shear rates, but decreases with increasing shear rate.

The zero-shear-rate viscosities are obtained by averaging the simulation data at the various values of the shear rate lying within the linear Newtonian plateau region. The dependency of the zero-shear-rate viscosities on molecular weights at 293 K is shown in Figure 4. An exponential increase of viscosity with increasing molecular weight is observed, in accordance with the Mark-Houwink equation. The line in Figure 4 was obtained by fitting the simulation data using the relation: $\mu = KM_w^{\alpha}$ [46]. Fitting the simulation data to this expression, we obtained $K = 3.74 \times 10^{-6}$ cP and $\alpha = 2.03$. The power index α is, to within statistical error, exactly equivalent to the known value of 2 for dilute solutions of rigid rods [47,48]. From the perspective of a dense liquid, however, it lies between the values of 1 and 3.4, which are characteristic of untangled and entangled linear polymers, respectively [47,48]. Since these PFPE chains are relatively stiff and short, it is highly unlikely that any entanglements exist at all. The entanglement of short hydrocarbon chains has been discussed by Kim et al. [35]. Therefore, we should not expect to observe a power-law index of 3.4. However, it seems evident that the discrepancy between the values of 2 and 1 is due to the rigidity of the PFPE chains, since experimental data of unentangled, shorter-chain polyethylenes follow this scaling law quite well with a power-law index of unity [49].

4.2.2 *Potential energy contributions of PFPE chains and* n*-alkane $C_{24}H_{50}$ under shear*

In the previous study [21], we discussed the changes in the contributions to the potential energy for $C_8F_{18}O_4$ as induced by shear. There were no significant alterations of the potential energy contributions for any of the different types of interactions: bond stretching, bond bending, bond torsion and intra- and inter-molecular non-bonded interactions. Here, we examined the changes in the potential energy terms for all four chain lengths. We found that all of the compounds shared a similar trend, and thus we present only the results for the longest PFPE, $C_{16}F_{34}O_8$. Furthermore, we compare the results between $C_{16}F_{34}O_8$ and a *n*-alkane, $C_{24}H_{50}$, of which both have 24 atoms in the backbone.

In Figure 5, the potential energy contributions are displayed as functions of Weissenberg number (*We*) for compounds $C_{16}F_{34}O_8$ at 293 K and linear hydrocarbon $C_{24}H_{50}$ at 333 K. The Weissenberg number is a dimensionless number defined as the product of the strain rate and the longest relaxation time of the material. We choose to plot the potential energy and many of the remaining properties vs. the Weissenberg number rather than the strain rate, because the simulations for different compounds have been run at different temperatures. Because the Weissenberg number is a function of the relaxation time of the molecule and the relaxation time is a function of temperature, this is an indirect way to account for the fact that the temperature varies among compounds. The relaxation times used in this work are

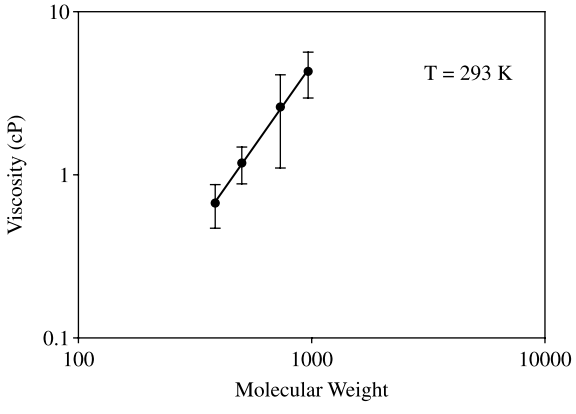

Figure 4. The zero-shear-rate viscosity vs. molecular weight at 293 K for compounds $C_6F_{14}O_3$, $C_8F_{18}O_4$, $C_{12}F_{26}O_6$, and $C_{16}F_{34}O_8$ using the revised UFF potential. The line is obtained by fitting the data to an exponential equation.

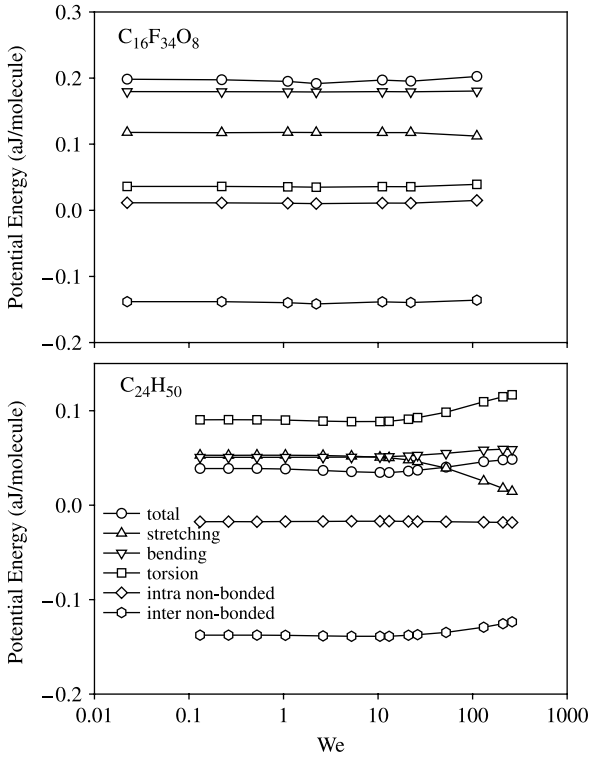

Figure 5. The contributions of the different interactions to the potential energy as functions of Weissenberg number for compounds $C_{16}F_{34}O_8$ at 293 K and $C_{24}H_{50}$ at 333 K.

188 ps for $C_{16}H_{34}$ at 323 K, 617 ps for $C_{24}H_{50}$ at 333 K, 883 ps for $C_{12}F_{26}O_6$ at 293 K and 2.22 ns for $C_{16}F_{34}O_8$ at 293 K.

Further justifying the comparison across temperatures is the fact that the data for $C_{16}F_{34}O_8$ at 373 K show similar trends to those at 293 K. Therefore, it is reasonable to compare results between $C_{16}F_{34}O_8$ at 293 K and $C_{24}H_{50}$ at 333 K. The detailed information for $C_{24}H_{50}$ has been published previously [32]. Here, we focus on the comparison between a stiff PFPE and a relatively flexible *n*-alkane. The position where *We* equals 1 usually defines the boundary between Newtonian and shear-thinning behaviour. From Figure 5, we observe for both compounds that the potential energy for intermolecular non-bonded interactions of both compounds is negative, indicating an attractive interaction between molecules. The intramolecular non-bonded interactions give a positive (repulsive) energy for $C_{16}F_{34}O_8$, and a negative (attractive) one for $C_{24}H_{50}$, which displays the effect of the large size difference between fluorine and hydrogen atoms. The fluorine atoms are large enough that those bound to contiguous carbon atoms repel each other to a much greater degree, thus creating a much more rigid monomeric unit, as well as a more rigid structure between adjacent monomers.

The potential energy does not alter substantially with Weissenberg number for the relatively inflexible $C_{16}F_{34}O_8$ chains, while there are noticeable changes for the more flexible $C_{24}H_{50}$. All of the energetic terms are relatively constant for about an order of magnitude of shear rate greater than the critical shear rate that represents the end of the Newtonian plateau. This observation is consistent with the hydrocarbon NEMD work of Baig et al. [33], which showed that simple linear relationships such as the stress-optical law remain valid to some shear rate beyond the critical shear rate. Beyond this point, we observe that the potential energy contribution due to bond stretching decreases. The decrease is very slight in the PFPE and substantially more pronounced in the hydrocarbon. At very high Weissenberg numbers, the flow induces a structure that can partially freeze out these high frequency vibrational modes, as has been shown previously from NEMD simulation for hydrocarbons in elongational flow [50]. This change in the bond stretching energy is thus a consequence of a more elongated chain configuration, which will be seen more clearly in the other energetic contributions. That the effect is greater in a hydrocarbon than in a PFPE is a direct consequence of the enhanced flexibility of the hydrocarbon chain, as the degree of structural elongation is more substantial.

The bond-bending energy contribution shows modest increases in both chains, but again is more substantial in the flexible chain. The torsion energy has previously been identified as one of the key components of flow-induced structural changes in hydrocarbons since it directly captures the transition from a distribution of gauche and trans-conformations to a distribution more weighted to trans-conformations as the chains extend in the flow. Again, the magnitude of the change is greater for the more flexible hydrocarbon. This flow-induced change in chain configuration affects both the intra- and inter-molecular non-bonded interactions. In both compounds, the intermolecular energy increases slightly in response to the conformation change. In the PFPE, we see a greater degree of change in the energy of the intramolecular non-bonded energy, since in the PFPE this is largely due to fluorine–fluorine repulsion, and is therefore more sensitive to small changes in chain configuration.

4.2.3 Configurational transformations of PFPE chains under shear

In Figure 6, an important structural quantity, the mean-square end-to-end distance of chains, $\langle R^2_{ete}\rangle$, is presented as a function of Weissenberg number for the compounds $C_{16}H_{34}$ at 323 K, $C_{24}H_{50}$ at 333 K, and $C_{12}F_{26}O_6$ and $C_{16}F_{34}O_8$ at 293 K. The analogous hydrocarbons have backbone lengths of 16 and 24 atoms. The PFPEs have backbone lengths of 18 and 24 atoms. In a prior publication [21], the temperature dependence of $\langle R^2_{ete}\rangle$ was presented. Here we focus on the dependence of $\langle R^2_{ete}\rangle$ on chain length and flexibility. The $\langle R^2_{ete}\rangle$ is used as one measure of the extension of a chain due to the application of the flow field. For short chains, which are typically relatively stiff and fairly extended at equilibrium, one expects to see very little extension due to flow. For longer chains, which are more tightly coiled at equilibrium, one expects to see much more significant flow-induced chain extension. For stiff chains, which coil to a lesser extent

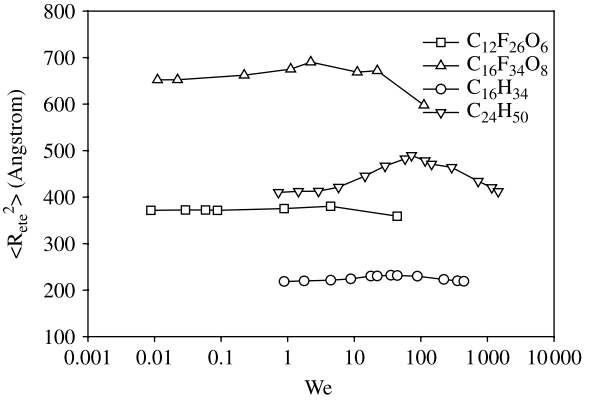

Figure 6. The dependence on Weissenberg number of the mean-square chain end-to-end distance, $\langle R^2_{ete}\rangle$, for the compounds $C_{16}H_{34}$ at 323 K, $C_{24}H_{50}$ at 333 K, and $C_{12}F_{26}O_6$, $C_{16}F_{34}O_8$ at 293 K.

at equilibrium, one would expect to see a smaller degree of flow-induced chain extension than for flexible chains.

In Figure 6, we plot the dependence on Weissenberg number of $\langle R^2_{ete} \rangle$ for the four compounds. For the shorter chains, $C_{12}F_{26}O_6$ and $C_{16}H_{34}$, the magnitude of the change of $\langle R^2_{ete} \rangle$ is less than 8%. As mentioned previously, the shorter chains are relatively more extended under quiescent conditions, and the shear field does not have a significant effect on the end-to-end distance. For the longer chains, $C_{16}F_{34}O_8$ and $C_{24}H_{50}$, the magnitude is larger, 15 and 20%, respectively. The PFPE, being much stiffer and thus more fully extended under quiescent conditions, experiences a smaller degree of extension than the more flexible hydrocarbon. For the shorter PFPE, $\langle R^2_{ete} \rangle$ remains nearly constant at low Weissenberg numbers, then slightly decreases at higher Weissenberg numbers. This reduction at high Weissenberg numbers is primarily due to the increased frequency of molecular rotation [35], which effectively shortens the end-to-end distance, on average, as the chain ends pass each other during the rotational period. A similar behaviour was reported for another short PFPE, $C_8F_{18}O_4$, in the previous work [21]. For the longer PFPE, the $\langle R^2_{ete} \rangle$ slightly increases at low Weissenberg numbers, then decreases at high Weissenberg numbers. This is due to the longer chain PFPE being relatively more flexible than the short chain PFPE, and therefore capable of extending more with increasing flow strength. However, at high Weissenberg numbers, molecular rotation begins to dominate and, as in the case of the shorter chain PFPE, the end-to-end distance decreases. As for the hydrocarbons, both show a maximum in $\langle R^2_{ete} \rangle$ at an intermediate value of the Weissenberg number. Since these chains are both fairly flexible, even the shorter chain hydrocarbon can extend to a small degree with increasing flow strength. The magnitude of the maximum is greater for the longer chain. A maximum in $\langle R^2_{ete} \rangle$ in *n*-alkanes undergoing shear flow has been previously observed in NEMD simulations [30,31]. The longer chain hydrocarbon experiences a greater degree of both extension at intermediate Weissenberg numbers and compression at high ones due to its enhanced flexibility: the chains can extend more at lower Weissenberg numbers and rotate with more ellipsoidal (rather than circular) configurations (thus bringing the chain ends closer together) at higher Weissenberg numbers [35].

In evaluating the effect of chain stiffness on the dependence of $\langle R^2_{ete} \rangle$ on Weissenberg number, we can compare the long PFPE and hydrocarbon, both of which have 24 backbone atoms. Moreover, CO and CC bond lengths are very similar; therefore, $C_{16}F_{34}O_8$ and $C_{24}H_{50}$ should have a similar $\langle R^2_{ete} \rangle$ if both compounds possess the same degree of chain flexibility. However, at equilibrium, $C_{16}F_{34}O_8$ and $C_{24}H_{50}$ have $\langle R^2_{ete} \rangle$ values of 652 and 410 Å^2, respectively: $C_{24}H_{50}$ has a smaller $\langle R^2_{ete} \rangle$ because of its greater degree of flexibility. In Figure 7, we show a snapshot of ten randomly chosen chains for both compounds at equilibrium. (We have rendered only ten chains for visual clarity within the dense liquid.) We see that the hydrocarbon molecules have many more gauche configurational torsion angles in them as compared to the PFPE molecules. Some PFPE chains do slightly bend, but the degree of folding is significantly higher for the hydrocarbon molecules. The stiffness of the chain is directly related to the torsion energy barrier; the smaller the torsion energy barrier, the higher the chain flexibility. In alkanes, the torsional (CCCC) energy barrier is about 4.8 kcal/mol [51] and the torsion energy barriers in $C_{16}F_{34}O_8$ are 6.6 and 5.7 kcal/mol for CCOC and OCCO, respectively [3,18].

The mean-square radius of gyration, $\langle R^2_g \rangle$, is a structural property that quantifies the mean-square length between all

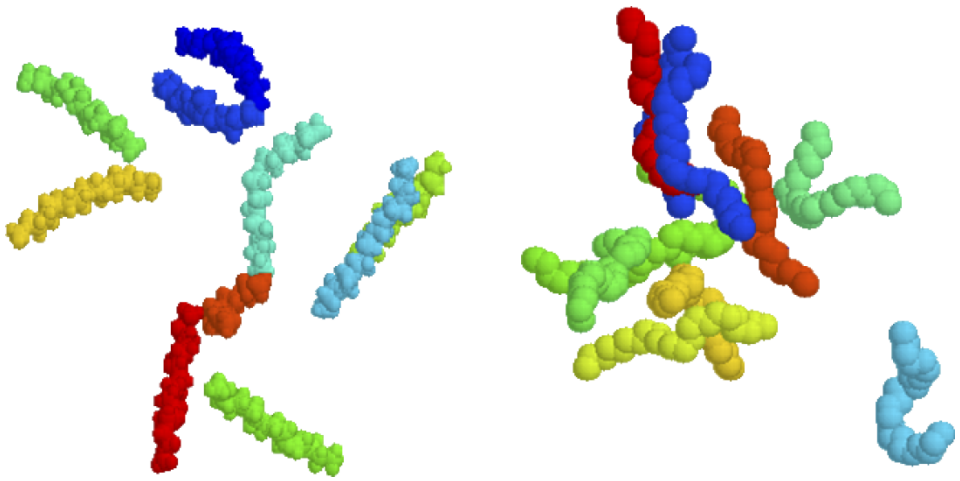

Figure 7. The snapshots of ten randomly chosen chains for $C_{16}F_{34}O_8$ (left) at 293 K and $C_{24}H_{50}$ (right) at 333 K under quiescent conditions. All other chains have been rendered invisible.

pairs of the atomic constituents of the chains. In Figure 8, we present the dependence on Weissenberg number of the ratio $\langle R^2_{ete}\rangle/\langle R^2_g\rangle$ for the same two alkanes and two PFPEs as discussed in Figure 6. Long, linear polymer chains typically display a $\langle R^2_{ete}\rangle/\langle R^2_g\rangle$ ratio of 6 [49]. For these four compounds, the ratio is much larger than 6, which is common for shorter chains, even those of *n*-alkanes [35]. Furthermore, the zero-shear-rate values for the PFPEs are substantially larger than those for the hydrocarbons, which can again probably be attributed to the relative stiffness of the former. For all four compounds, the $\langle R^2_{ete}\rangle/\langle R^2_g\rangle$ ratio is constant at low Weissenberg numbers, and increases until reaching a maximum, and then decreases. Both hydrocarbon compounds have a much more pronounced increase than their corresponding PFPE counterparts. The increase of the $\langle R^2_{ete}\rangle/\langle R^2_g\rangle$ ratio is mainly caused by the extension of chains, due to the definitions of $\mathbf{R}_{ete}$ and $\mathbf{R}_g$. The extension of chain will increase both $\langle R^2_{ete}\rangle$ and $\langle R^2_g\rangle$, but $\langle R^2_{ete}\rangle$ is by definition a much stronger function of the end-to-end distance, so that $\langle R^2_{ete}\rangle$ increases with chain extension much more than $\langle R^2_g\rangle$. Comparison between Figures 6 and 8 demonstrates that the maxima of $\langle R^2_g\rangle$ and $\langle R^2_{ete}\rangle/\langle R^2_g\rangle$ coincide. The magnitude of variation quantifies the flexibility of the chains, again demonstrating that the two hydrocarbon chains have a higher degree of flexibility than their PFPE counterparts with similar chain length. At high values of the shear rate, the ratio decreases as the chain end-to-end vectors decrease due to the increased frequency of rotation, as described above.

4.2.4 The dependence of normalised conformation tensor on the shear rate

The normalised conformation tensor is defined as $C \equiv 3\langle \mathbf{R}_{ete}\mathbf{R}_{ete}\rangle/\langle R^2_{ete}\rangle_{eq}$, where the denominator is evaluated under equilibrium conditions. The conformation tensor provides a macroscopic quantification of molecular-scale chain configurations, and serves as the principal conformational variable in many continuum formulations of viscoelastic fluid behaviour. Under quiescent conditions, all diagonal components of $\mathbf{C}$ assume the unit value, and all off-diagonal elements vanish. In Figure 9, we plot the non-zero components of the normalised conformation tensor as functions of Weissenberg number for the same two PFPEs and two hydrocarbons discussed above. The conformation tensors for $C_{16}H_{34}$ and $C_{24}H_{50}$ can also be found in [35]. In this study, x is the flow direction, y is the direction of the velocity gradient and z is the neutral direction. All four compounds demonstrate similar trends for all components of the normalised conformation tensor as functions of Weissenberg number. C_{xy} slowly increases at low Weissenberg numbers, then rapidly increases at intermediate values until attaining a plateau and experiencing a gradual decrease thereafter. This component contains information regarding both extension and orientation of the molecular chains. The extensional contribution follows the same qualitative trend as $\langle R^2_{ete}\rangle$; however, the orientational contribution eventually plateaus at high Weissenberg numbers as the average orientation angle approaches 0° (Figure 10). This decrease in C_{xy} at high Weissenberg numbers has been noted before in NEMD simulations [33], and is very interesting because in many viscoelastic models it implies a decrease in the shear stress under these conditions, which is an apparently aphysical result. This seems to indicate that the relationship between shear stress and conformation tensor in many viscoelastic fluid models is incomplete at high Weissenberg numbers. This is most likely due to the neglect of the significant rotational effects occurring at very high Weissenberg numbers.

The conformation tensor component C_{xx} is primarily associated with the extension of the molecular chains, as evidenced by the close coupling of the data of Figure 9 with those of $\langle R^2_{ete}\rangle$, discussed above. This component attains a maximum at the same value of the shear rate as the mean-square end-to-end distance, and decreases thereafter for exactly the same reasons. The components C_{yy} and C_{zz} decrease with increasing Weissenberg numbers, in response to the extension of the chains in the x direction. This decrease is due to the compression of the chains in the directions perpendicular to the direction of elongation. Both the PFPEs and hydrocarbons experience the same degree of compression, indicating that this effect is too small to register as a function of the degree of flexibility.

In Figure 10, we plot the alignment angle as a function of Weissenberg number for the two PFPEs and two alkanes discussed above. We observe that the alignment angle exhibits its theoretical limiting values of 45° at small Weissenberg numbers, and decreases rapidly with increasing Weissenberg number. At extremely high Weissenberg numbers, the alignment angle reaches

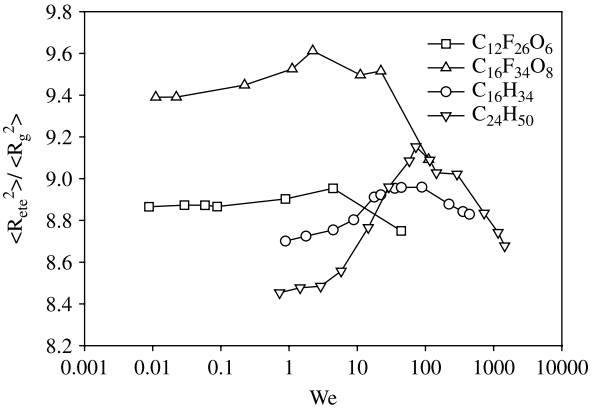

Figure 8. The dependence on Weissenberg number of the ratio $\langle R^2_{ete}\rangle/\langle R^2_g\rangle$ for compounds $C_{16}H_{34}$ at 323 K, $C_{24}H_{50}$ at 333 K, and $C_{12}F_{26}O_6$, $C_{16}F_{34}O_8$ at 293 K.

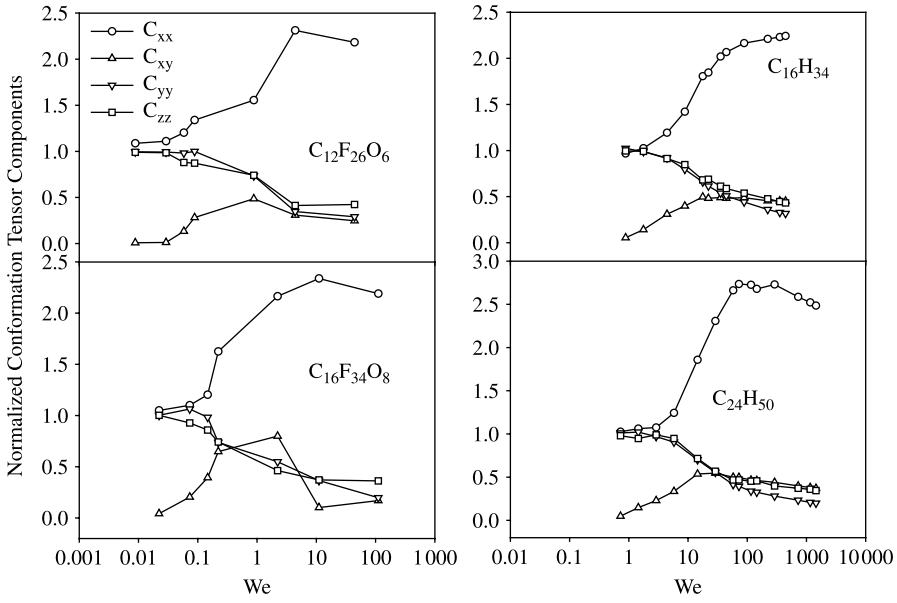

Figure 9. The dependence on Weissenberg number of the normalised conformational tensor components for compounds $C_{16}H_{34}$ at 323 K, $C_{24}H_{50}$ at 333 K, and $C_{12}F_{26}O_6$, $C_{16}F_{34}O_8$ at 293 K.

a plateau value of about 5°, which is a typical value for polymeric fluids under shear. For both the stiff PFPEs and the flexible alkanes, the final alignment angle is smaller for the longer chains, as these molecules experience a greater degree of average alignment in the flow direction due to a relative decrease in the frequency of rotation. We also see that the stiffer PFPEs have a smaller final alignment angle than their alkane counterparts, which seems to imply that the rotational rates are lower for the relatively stiff PFPE chains, as noted above.

Taking the energetic and structural properties as a whole, we can come to a general understanding of the role of chain flexibility in these systems. At one end of the spectrum of chain flexibility, the chains are rigid rods. Rigid rods respond to a flow field strictly via alignment of rods; there is no component of rod extension. At the other end of the spectrum are fully flexible chains, which can both align and extend. PFPEs and alkanes fall within this spectrum, but the PFPEs exhibit the characteristics of much stiffer chains than the *n*-alkanes. Alkanes respond to the flow field with a combination of alignment and extension. PFPEs respond with greater alignment but less extension. This extension is caused by configurational changes of the chain constituent atomic units. Therefore, the contributions to the potential energy in the relatively flexible alkanes change to a greater extent as a result of the flow field than is true for the relatively rigid PFPEs. In these systems, we find that the maximum degree of alignment is greater for the rigid PFPEs than for an alkane of corresponding backbone length.

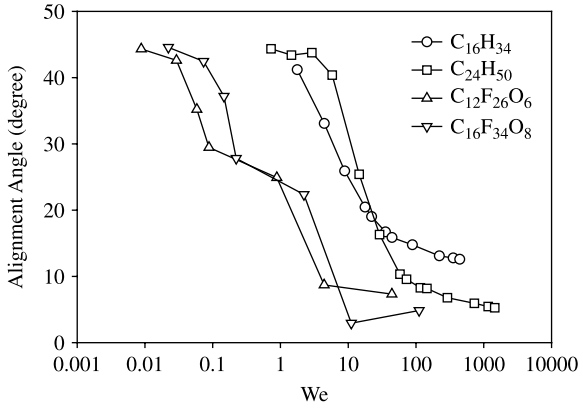

Figure 10. The dependence on Weissenberg number of alignment angle for compounds $C_{16}H_{34}$ at 323 K, $C_{24}H_{50}$ at 333 K, and $C_{12}F_{26}O_6$, $C_{16}F_{34}O_8$ at 293 K.

5. Conclusions

We have reported shear viscosities for seven PFPE compounds from NEMD simulation and from experiment. The full parameter set for linear PFPE of a revised UFF with multiple types of fluorine atoms is presented. By measuring the viscosity of PFPE with different architectural elements both experimentally and in simulation, we can arrive at several general statements regarding the relationship between viscosity and PFPE architecture. First, longer chain backbone lengths increase the viscosity. Second, ether linkages in the backbone decrease the viscosity. Third, longer $(CF_2)_n$ units between ether linkages

increase the viscosity. These effects can all be explained in terms of chain flexibility. The large fluorine atoms create a relatively high-energy barrier for torsional motion required to change from a gauche to trans conformations. The presence of the oxygen significantly reduces this energy barrier. The strategic placement of oxygen in the chain backbone defines the size of the monomeric units and results in the ability to control of the viscosity of compounds that have the same chemical formula.

Additionally, we reported the structural and rheological properties of four short-chain PFPEs with common monomeric units but of varying chain length using NEMD simulation of PCF. We found a power-law index relating viscosity to chain length of 2, which is generally characteristic of rigid chain molecules. From the alignment angle, we observed that longer chains align to a greater degree in shear flow, as expected. We also saw that longer chains have a more pronounced maximum in the end-to-end distance as a function of Weissenberg numbers, indicating that longer chains are capable of greater extension (increasing the end-to-end distance at low Weissenberg numbers) and are more susceptible to rotational phenomena (decreasing the average end-to-end distance at high Weissenberg numbers). These observations are commensurate with the conceptual understanding that longer chains have a greater relative flexibility.

Finally, we provided a quantitative comparison of the structural and energetic properties of relatively rigid PFPEs and relatively flexible alkanes as functions of chain length. From the end-to-end distance, we found that following the same argument regarding chain flexibility, alkanes show a more pronounced maximum in the end-to-end distance as a function of Weissenberg number. From the alignment angle, we observed that the rigid PFPEs align to a greater extent than flexible alkanes, which also is reasonable based on arguments of relative chain flexibility. The conformation tensors for the PFPEs and alkanes are qualitatively similar. The increase in C_{xx} and the decrease in C_{yy} and C_{zz} correspond to alignment of the chains in the flow direction. In PFPEs, the alignment of rigid chains is the primary mechanism, whereas in the more flexible alkanes, there is a more substantial element of chain extension that complements chain alignment. In all cases, we observed that C_{xy} attains a maximum at lower Weissenberg number values than C_{xx}, which suggests that there may be different relaxation times associated with chain extension (captured in C_{xx}) and chain rotation (captured in C_{xy}).

Acknowledgements

This research has been supported by the Air Force Office of Scientific Research through contract # FA 9550-05-1-0342. Through the University of Tennessee Computational Science Initiative, the authors used resources of the Center for Computational Sciences at Oak Ridge National Laboratory, which is supported by the Office of Science of the DOE under Contract DE-AC05-00OR22725. The authors acknowledge the experimental synthesis and helpful discussions of Dr Jamie Adcock in the Department of Chemistry at University of Tennessee, Knoxville. The authors also acknowledge discussions of Dr Chunggi Baig in the Department of Chemical Engineering at the University of Patras, Greece.

References

[1] L.S. Helmick et al., *The effect of humidity on the wear behavior of bearing steels with R_fO(n-$C_3F_6O)_xR_f$ perfluoropolyalkylether fluids and formulations*, Trib. Trans. 40 (1997), p. 393.

[2] G.A. Bell, J. Howell, and T.W. Del Pesco, *Perfluoroalkylpolyethers*, in *Synthetic Lubricants and High-Performance Functional Fluids*, L.R. Rudnick and R.L. Shubkin, eds., Marcel Dekker, Inc., New York, 1999, p. 215.

[3] H.-C. Li et al., *Development of a force field for molecular simulation of the phase equilibria of perfluoro-methyl-propyl ether*, Mol. Phys. 100 (2002), p. 265.

[4] F. Sadeghi, E.J. Trope, and T.J. Schnell, *Performance characteristics of perfluoroalkylpolyether synthetic lubricants*, Trib. Trans. 39 (1996), p. 849.

[5] C.E. Snyder, Jr., L.J. Gschwender, and O.L. Scott, *Characterization of model perfluoropolyalkylethers by miniaturized thermal oxidative thechniques-part II: pressure differential scanning calorimetry*, Trib. Trans. 38 (1995), p. 733.

[6] L.J. Gschwender et al., *The effect of additives on the wear behavior of bearing steels with $R_fO(CF_2O)_x(CF_2CF_2O)y(CF_2$-$CF_2CF_2O)_zR_f$ perfluoropolyalkylether fluids*, Trib. Trans. 41 (1998), p. 78.

[7] K.S. Mriziq, M.D. Dadmun, and H.D. Cochran, *Rheology and birefringence of Fomblin YR at very high shear rates*, Rheol. Acta 46 (2007), p. 839.

[8] Q. Guo et al., *Surface morphology and molecular conformation for ultrathin lubricant films with functional end groups*, J. Appl. Phys. 93 (2003), p. 8707.

[9] Y. Tanaka et al., *Density and viscosity of linear perfluoropolyethers under high-pressures*, Int. J. Thermophysics 10 (1989), p. 857.

[10] R.N. Kono et al., *Rheology of perfluoropolyether lubricants*, IEEE Trans. Magn. 37 (2001), p. 1827.

[11] A. Koike, *Molecular dynamics study of tribological behavior of confined branched and linear perfluoropolyethers*, J. Phys. Chem. B 103 (1999), p. 4578.

[12] Q. Guo et al., *Molecular rheology of perfluoropolyether lubricant via nonequilibrium molecular dynamics simulation*, J. Appl. Phys. 99 (2006), p. 08N105.

[13] Q. Guo et al., *Transport properties of nanoscale lubricant films*, IEEE Trans. Magn. 40 (2004), p. 3177.

[14] K.S. Mriziq et al., *High-shear rate optical rheometer*, Rev. Sci. Instrum. 75 (2004), p. 2171.

[15] M.S. Jhon, *Physicochemical properties of nanostructrured perfluoropolyether films*, in *Advances in Chemical Physics*, S.A. Rice, ed., John Wiley and Sons, Inc., 2004, Vol. 129, p. 1.

[16] X. Li, Y.-Z. Hu, and H. Wang, *A molecular dynamics study of lubricant perfluoropolyther in hard disk driver*, Acta Phys. Sinica 54 (2005), p. 3787.

[17] H.-C. Li, *Molecular modeling of perfluoro compounds*, Ph.D. diss., University of Tennessee, Knoxville, 2001.

[18] H.-C. Li et al., *On the development of a general force field for the molecular simulation of perfuoropolyethers*, Mol. Phys. 101 (2003), p. 2157.

[19] D. Kamei et al., *Computational chemistry study on the dynamics of lubricant molecules under shear conditions*, Tribol. Int. 36 (2003), p. 297.

[20] S. Senapati and M.L. Berkowitz, *Molecular dynamics simulation studies of polyether and perfluoropolyether surfactant based*

reverse micelles in supercritical carbon dioxide, J. Phys. Chem. B 107 (2003), p. 12906.
[21] B. Jiang, D.J. Keffer, and B.J. Edwards, *Estimation and analysis of the rheological properties of a perfluoropolyether through molecular dynamics simulation*, J. Fluorine Chem. 127 (2006), p. 787.
[22] B. Jiang et al., *Comparison of rheological properties of short-chain perfluoropolyethers through simulation and experiment*, Mol. Simul. 33 (2007), p. 871.
[23] C. McCabe et al., *Transport properties of perfluoroalkane using molecular dynamics simulation: comparison of united- and explicit-atom models*, Ind. Eng. Chem. Res. (2003), p. 42.
[24] A.K. Rappe et al., *UFF, a full periodic table force field for molecular mechanics and molecular dynamics simulations*, J. Am. Chem. Soc. 114 (1992), p. 10024.
[25] C. Baig et al., *A comparison of simple rheological models and simulation data of* n*-hexadecane under shear and elongational flows*, J. Rheol. 50 (2006), p. 625.
[26] ———, *Rheological and structural studies of linear polyethylene melts under planar elongational flow using nonequilibrium molecular dynamics simulations*, J. Chem. Phys. 124 (2006), p. 084902.
[27] ———, *Rheological and structural studies of liquid decane, hexadecane, and tetrasosane under planar elongational flow using nonequilibrium molecular dynamics simulations*, J. Chem. Phys. 122 (2005), p. 184906.
[28] S.T. Cui, P.T. Cummings, and H.D. Cochran, *Multiple time step nonequilibrium molecular dynamics simulation of the rheological properties of liquid* n*-decane*, J. Chem. Phys. 104 (1996), p. 255.
[29] S.T. Cui, S.A. Gupta, and P.T. Cummings, *Molecular dynamics simulations of the rheology of normal decane, hexadecane, and tetracosane*, J. Chem. Phys. 105 (1996), p. 1214.
[30] J.D. Moore et al., *A molecular dynamics study of a short-chain polythylene melt. I. Steady-state shear*, J. Non-Newtonian Fluid Mech. 93 (2000), p. 83.
[31] ———, *A molecular dynamics study of a short-chain polythylene melt. II. Transient response*, J. Non-Newtonian Fluid Mech. 93 (2000), p. 101.
[32] J.M. Kim, D.J. Keffer, M. Kröger and B.J. Edwards, *Rheological and entanglement characteristics of linear chain polyethylene liquids in planar couette and planar elongational flows*, J. Rheol. (2007) in press.
[33] C. Baig, B.J. Edwards, and D.J. Keffer, *A molecular dynamics study of the stress-optical behavior of a linear short-chain polyethylene melt under shear*, Rheol. Acta 46 (2007), p. 1171.
[34] C. Baig, *Studies in rheology: molecular simulation and theory*, Ph.D. diss., University of Tennessee, Knoxville, August, 2005.
[35] J.M. Kim, D.J. Keffer, B.J. Edwards, and C. Baig, *Visualization of conformational changes of linear alkanes and short polyethylenes under shear and elongational flows*, J. Mol. Graph. Mod. (2007), doi: 10.1016/j.jmgm.2007.09.001.
[36] J.L. Adcock and M.L. Cherry, *Aerosol direct fluorination: direct synthesis of perfluorinated glyme ethers*, J. Fluorine Chem. 30 (1985), p. 343.
[37] ———, *Aerosol direct fluorination: a developing synthesis technology and an entry level mechanistic tool. A short review*, Ind. Eng. Chem. Res. 26 (1987), p. 208.
[38] J.L. Adcock, K. Horita, and E.B. Renk, *Low-temperature fluorination of aerosol suspensions of hydrocarbons utilizing elemental fluorine*, J. Am. Chem. Soc. 103 (1981), p. 6937.
[39] W.G. Hoover, *Canonical dynamics: equilibrium phase-space distributions*, Phys. Rev. A 31 (1985), p. 1695.
[40] S. Nosé, *A unified formulation of the constant temperature molecular dynamics methods*, J. Chem. Phys. 81 (1984), p. 511.
[41] M. Tuckerman, B.J. Berne, and G.J. Martyna, *Reversible multiple time scale molecular dynamics*, J. Chem. Phys. 97 (1992), p. 1990.
[42] K.P. Travis and D.J. Evans, *On the rheology of* n*-eicosane*, Mol. Simul. 17 (1996), p. 157.
[43] J. Delhommelle and D.J. Evans, *Correspondence between configurational temperature and molecular kinetic temperature thermostats*, J. Chem. Phys. 117 (2002), p. 6016.
[44] D.J. Evans and G.P. Morris, *Statistical Mechanics of Nonequilibrium Liquids*, Academic Press, New York, 1990.
[45] A.W. Lees and S.F. Edwards, *Computer study of transport processes under extreme conditions*, J. Phys. C Solid 5 (1972), p. 1921.
[46] P. de Gennes, *Scaling Concepts in Polymer Physics*, Cornell University, Ithaca, NY, 1979, p. 241.
[47] R.B. Bird, R.C. Armstrong, and O. Hassager, *Dynamics of polymeric liquids*, *Fluid Dynamics*, Vol. 1, John Wiley & Sons, Inc., New York, 1987.
[48] R.B. Bird et al., *Dynamics of polymeric liquids*, *Kinetic Theory*, Vol. 2, John Wiley and Sons, Inc., New York, 1987.
[49] M. Doi, *Introduction to Polymer Physics*, Oxford University Press, New York, 1996.
[50] T.C. Ionescu et al., *Structure formation under steady-state isothermal planar elongational flow of* n*-eicosane: a comparison between simulation and experiment*, Phys. Rev. Lett. 96 (2006), p. 037802.
[51] W.L. Jorgensen, J.D. Madura, and C.J. Swenson, *Optimized intermolecular potential functions for liquid hydrocarbons*, J. Am. Chem. Soc. 106 (1984), p. 6638.